NTHAS7: The Seventh Korea-Japan Symposium on Nuclear Thermal Hydraulics and Safety
Chuncheon, Korea, November 14- 17, 2010

Paper Number N7P0028

NUMERICAL STUDY ON SODIUM DYNAMICS NEAR REACTION SURFACE IN COUNTERFLOW OF SODIUM AND WATER VAPOR

Joji SOGABE[1*], Akira YAMAGUCHI[1], Takashi TAKATA[1]
Hiroyuki OHSHIMA[2], Shin KIKUCHI[2]

[1] Graduate School of Engineering, Osaka University,
2-1, Yamada, Suita, Osaka, Japan, 565-0871,
+81-6-6879-7895, sogabe_j@qe.see.eng.osaka-u.ac.jp;
yamaguchi@see.eng.osaka-u.ac.jp; takata_t@see.eng.osaka-u.ac.jp

[2] Japan Atomic Energy Agency
4002, Narita, O-arai, Ibaraki, Japan, 311-1393

ABSTRACT

Sodium water reaction (SWR) is a design basis accident of a sodium-cooled fast reactor (SFR). When a heat transfer tube fails, highly pressurized water or water vapor will leak into liquid sodium resulting in a chemical reaction between sodium and water or water vapor.

In the previous works, the mechanism of the SWR was researched on surface reaction and gas phase reaction. In gas phase reaction, the mechanism of the SWR especially at the reaction surface is complicated and has not been fully understood. The authors have developed a numerical code in which the chemical reaction model of sodium and water vapor is coupled with thermal-hydraulics. A SWR experiment of a counter-flow diffusion flame (in the gas phase) has also been carried out.

In the present paper, a numerical analysis of sodium dynamics near the reaction surface has been carried out based on the experimental result. It will be concluded that some of gas-phase sodium will absorb on aerosols generated in the SWR resulting in an exponentially decrease of gas-phase sodium concentration in the experiment.

1. INTRODUCTION

In a steam generator (SG) of a sodium-cooled fast reactor (SFR), liquid sodium and water and/or water vapor exchange the heat energy via heat transfer tubes. Liquid sodium has good properties of a high heat conduction coefficient and a high boiling point (1153K at atmospheric pressure) as a heat transport fluid. On the other hand, sodium has high chemical reactivity. When a heat transfer tube fails, highly pressurized water will leak into liquid sodium resulting in the following chemical reactions between sodium and water.

$$Na + H_2O \rightarrow NaOH + \frac{1}{2}H_2 \quad (1)$$

and

$$2Na + H_2O \rightarrow Na_2O + H_2 \quad (2)$$

Those phenomena are called as a sodium water reaction (SWR), which is a design basis accident of the SFR. Figure 1 shows a sketch of the SWR. Under the SWR condition, a deterioration of mechanical strength at high temperature (designated as an overheating rupture) and/or high alkali corrosion-erosion (designated as a wastage) might take place at the surface of the adjacent heat transfer tube. Thus, an estimation of the SWR phenomenon is of importance in order to understand safety design bases of the SG.

In the previous work, Takata and Yamaguchi (2005, 2009) proposed two SWR models and validated that those models are applicable to the coupling phenomena of the SWR. One is a surface reaction model, which assumes that water vapor reacts with liquid sodium. When liquid sodium vaporizes due to chemical reaction, the SWR shifts to the other mode, i.e. gas-phase reaction. In a gas-phase reaction, water vapor reacts with sodium gas. With regard to the chemical reaction between sodium and water in the gas phase, the elementary reaction and the reaction rate have not been fully understood.

In the present paper, the authors have developed a numerical code in which the chemical reaction model of sodium and water vapor is coupled with thermal-hydraulics. An SWR experiment of a counter-flow diffusion flame (in the gas phase) has also been carried out (Yamaguchi and Takata, et al., 2006, 2008). Comparing the experimental results with the numerical results, a numerical analysis of sodium dynamics near the reaction surface has been carried out based on the

experimental result.

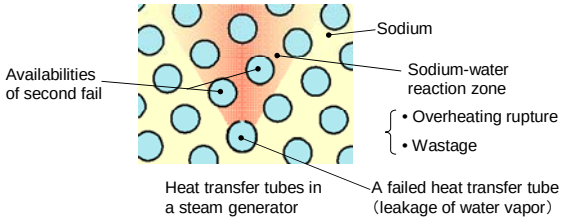

Fig. 1. Sketch of the sodium-water reaction

2. Computational Models

In this section, the computer models built in the developed code are briefly explained. In the computer program, SIMPLE (Semi-Implicit Method for Pressure-Linked Equations) algorithm is employed. Navier-Stokes equations and chemical reaction equations are solved interactively. In addition, a dynamic equation of aerosols is solved, coupled with the basic equations of thermal hydraulics. The source of the aerosols is the chemical products, i.e. sodium hydroxide and sodium oxide.

2.1 Governing Equations

Two-dimensional cylindrical coordinates are adopted considering the experimental apparatus. Governing equations for thermal hydraulics, i.e. the conservation equations of mass, momentum (in radial and axial directions), chemical species, energy, in the following:

$$\frac{\partial \rho}{\partial t}+\frac{1}{r}\frac{\partial}{\partial r}(\rho r u)+\frac{\partial}{\partial z}(\rho w)=\sum_j \left.\frac{\partial(\rho Y_j)}{\partial t}\right|_{react}, \quad (3)$$

$$\frac{\partial(\rho u)}{\partial t}+u\frac{\partial(\rho u)}{\partial r}+w\frac{\partial(\rho u)}{\partial z} =-\frac{\partial p}{\partial r}+\frac{1}{r}\frac{\partial}{\partial r}\left(r\mu\frac{\partial u}{\partial r}\right)+\frac{\partial}{\partial z}\left(\mu\frac{\partial u}{\partial z}\right), \quad (4)$$

$$\frac{\partial(\rho w)}{\partial t}+u\frac{\partial(\rho w)}{\partial r}+w\frac{\partial(\rho w)}{\partial z} =-\frac{\partial p}{\partial z}+\frac{1}{r}\frac{\partial}{\partial r}\left(r\mu\frac{\partial w}{\partial r}\right)+\frac{\partial}{\partial z}\left(\mu\frac{\partial w}{\partial z}\right)+\rho g, \quad (5)$$

$$\frac{\partial(\rho Y_j)}{\partial t}+\frac{1}{r}\frac{\partial(ru\rho Y_j)}{\partial r}+\frac{\partial(w\rho Y_j)}{\partial z} =\frac{1}{r}\frac{\partial}{\partial r}\left(r\rho D_j\frac{\partial Y_j}{\partial r}\right)+\frac{\partial}{\partial z}\left(\rho D_j\frac{\partial Y_j}{\partial z}\right)+\left.\frac{\partial(\rho Y_j)}{\partial t}\right|_{react}, \quad (6)$$

$$\frac{\partial(\rho C_p T)}{\partial t}+u\frac{\partial(\rho C_p T)}{\partial r}+w\frac{\partial(\rho C_p T)}{\partial z} =\frac{1}{r}\frac{\partial}{\partial r}\left(r\lambda\frac{\partial T}{\partial r}\right)+\frac{\partial}{\partial z}\left(\lambda\frac{\partial T}{\partial z}\right)+Q_D+Q_R, \quad (7)$$

where ρ, p and T are gas density, pressure and temperature, respectively. u and w are the velocity components in radial and vertical directions. Y_j and D_j are the mass fraction and the diffusion coefficient of chemical species j. μ, λ and C_p are the viscosity coefficient, the thermal conductivity and the specific heat at constant pressure, respectively. The right hand side of Eq. (3) expresses the mass production or consumption by the chemical reaction. The third term and the fourth term in the right hand side of Eq. (7) represent energy transferred by diffusion and heat generation of the chemical reactions, respectively.

2.2 Aerosol Dynamics

It is assumed that the water vapor reacts with sodium gas resulting in the emission of reaction products, i.e. sodium hydroxide and sodium oxide. Thus, the behavior of these levitating aerosols should be evaluated. In the computer program, aerosol dynamics is calculated such aerosol processes as coagulation, deposition and additional sources, which is discussed below. With respect to the dynamics of the spatially homogeneous particulate system, the evolution of a size distribution is described by the following general dynamic equation.

$$\frac{\partial n(v)}{\partial t}+div\left(\frac{n(v)}{C_u(v)}\mathbf{u}\right)+div\left(n(v)\mathbf{U}\right) =\frac{1}{2}\int_0^v n(v')n(v-v')\beta(v',v-v')dv' -n(v)\int_0^\infty n(v')\beta(v,v')dv'+S(v), \quad (8)$$

where $n(v)$ is the number density of the aerosol with its volume v. v' is a dummy variable that goes 0 to ∞ in the integration terms. β and S are the coagulation rate and the production term by the chemical reactions, respectively. $\mathbf{u}$ and $\mathbf{U}$ are the velocity vector and the terminal velocity vector, respectively.

The first term of the right hand side of Eq. (8) represents that the aerosol of volume v' coagulates with that of volume v-v' resulting in generating that of volume v. Likewise, the second term of the right hand side of Eq. (8) represents that the aerosol of volume v coagulate with that of volume v' resulting in generation of that of volume v+v'. It is assumed that aerosol coagulations are attributed to the Brownian diffusion, gravity, and turbulent flow. Mathematical expression for each coagulation rate β is given by Mitsutsuka (1984) and is not mentioned here. The production rate of the aerosol is based on the chemical reaction rate obtained in other routine. The diameter of the produced aerosol is assumed to follow a log-normal distribution.

The second term in the left hand side of Eq. (8) represents the advection due to the gas convection. Considering that a slip effect of aerosol and gas, the aerosol velocity can be set to the value divided gas velocity by the Cunningham correction factor C. The third term in the left hand side of Eq. (8) represents a mass transfer caused by applied forces to the aerosols such as deposition. The effect of the deposition is assumed that the summation of the Brownian diffusion, gravity settling, and thermophoresis.

2.3 Chemical Reaction Models

Two gas-phase chemical reaction models of water vapor and sodium gas are considered. One is the chemical equilibrium model in which instantaneous chemical equilibrium is assumed in this model (the reaction rate is infinite). Gibbs free energy minimization method is used. Na, H_2O, H_2 as gas components and NaOH, Na_2O, Na_2O_2 as reaction products are considered in the chemical equilibrium model. The concrete method of the model is given by Okano (1999).

The other is the Arrhenius law type model that takes the transient state into consideration (designed as Arrhenius model). The reaction rate is finite. With regard to the reaction path, it is assumed that the chemical reaction of producing sodium hydroxide is dominant. In a report of Takata and Yamaguchi (2005), the mechanisms of the gas-phase reaction are investigated using an ab initio molecular orbital (MO) method. According to the report, the energy barrier to activate the reaction described by Eq. (1) and Eq. (2) is 201kJ/mol and 326.5kJ/mol, respectively. Thus, it is considered that the chemical reaction described by Eq. (1) is dominant and sodium hydroxide is mainly produced in the SWR phenomenon. In the Arrhenius model, it is assumed that only Eq. (1) takes place based on the MO method or the energy barrier. The reaction rate is generally described as:

$$\gamma_{Na} = -k[Na][H_2O] \ , \qquad (9)$$

where k is the reaction rate constant. [•] means the molecular concentration of the reactant. According to the Arrhenius law, the reaction rate constant k is estimated by:

$$k = AT^m \exp\left(-\frac{E}{RT}\right) , \qquad (10)$$

where A, R, T and E are the frequency factor, the gas constant, temperature, and the activation energy, respectively.

3. Counterflow Diffusion Flame Experiment and Numerical Simulation

To understand the SWR phenomena and to validate the numerical simulation method, a counterflow diffusion flame experiment has been carried out (Yamaguchi and Takata, et al., 2006, 2008). An experimental apparatus is shown in Fig. 2. The configuration of the apparatus is an axial symmetrical cylinder.

The outline of the experiment is as follows. There is a 30mm-diameter sodium pool in the lower side of the apparatus, in which heated liquid sodium exists. From the upper side of the apparatus, water vapor diluted by argon gas was blown off to the sodium pool. From the pool, the saturated sodium gas rises and encounters with the water vapor. Hence, the SWR takes place and a counterflow diffusion flame is formed between the pool surface and the flow nozzle. Here, it is noted that a reaction surface location almost corresponds to a flame location where sodium emits itself. Two guard flows around the pool are adjusted to form an optimal flow field and temperature field for continuous chemical reaction and clear visualization and measurement.

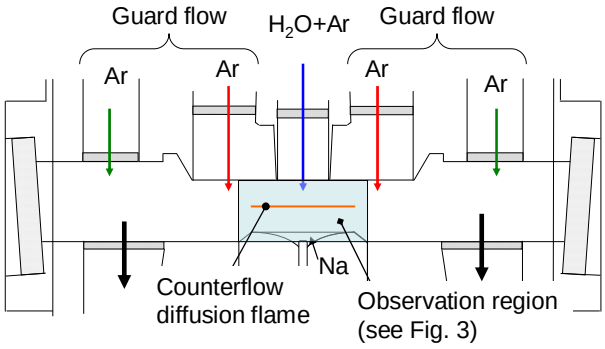

Fig. 2. Experiment apparatus of counterflow diffusion flame

3.1 Experiment in Low-Pressure Condition

In the experiment reported by YAMAGUCHI and TAKATA (2006), the flame location was very low (0.3mm above from the pool surface) and the chemical quantities around the reaction surface were not clearly measured.

Yamaguchi and Takata (2008) proposed an experiment in low-pressure condition. It is expected that the flame moves upward and reaction region became thicker because of the decrease of the reactant gas density in low-pressure condition. Moving upward and thickening of reaction region lead to sophisticate the measurement accuracy of the thermal hydraulic and chemical quantities. The flame location is influenced by the relationship of the water vapor and sodium gas mass flux. To lift up the location, either increasing the mass flux or decreasing the water vapor mass flux. They calculated the counterflow diffusion reaction area in low-pressure condition and confirmed that the flame location raised and reaction region enlarged.

Experiments in low-pressure condition referred to the numerical results are carried out. Experimental conditions are as follows. Pressure and the sodium pool temperature are 0.042MPa and 820K, respectively. The water vapor concentration and velocity are 2.0 volumetric percent and 0.11m/s, respectively. The

experimental conditions are summarized in Table 1. A picture taken around the reaction surface in the experiment is shown in Fig. 3. Indeed, in the low-pressure condition, as shown in Fig. 3, the flame location (=the reaction surface location) moved upward (10mm from the pool surface) and the reaction area enlarged. The low-pressure experiment enabled the authors to enhance the measurement accuracy of chemical species concentration and temperature field.

Table 1. Experimental conditions

Pressure	Pool temperature	Velocity	Water Vapor
0.042MPa	820K	0.11m/s	2.0vol%

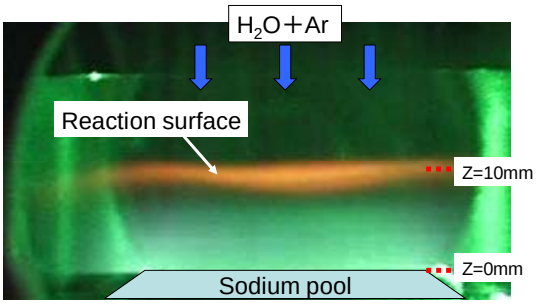

Fig. 3. Counterflow Diffusion Flame Experiment

3.2 Numerical Simulations in Accordance with the Condition of the Low-Pressure Experiment

Numerical simulations in the low-pressure experimental condition are performed, i.e. numerical conditions such as pressure, the pool temperature, water vapor concentration and velocity are the same as the experiments. The influence of the chemical reaction models are investigated by comparing two types: the chemical equilibrium model and the Arrhenius model. When Arrhenius model is adopted, the rate constant k (described in Eq. (10)) is set to constant value of 10^6 [m^3/mol/s]. The detail of the models is described in section 2.3.

Figure 4 shows volume concentration distributions of sodium and water vapor of the experimental and the numerical results. It can be said that the reaction surface

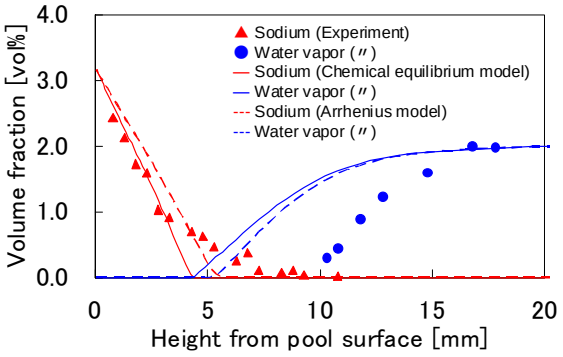

Fig. 4. Sodium and water vapor concentration distributions near reaction surface

exists where the reactants such as sodium vapor and water vapor disappear. At a glance, it is found that the reaction surface locations are different between the experiment and the simulation. The reaction surface of the former is near 10mm above the pool surface and this corresponds to the flame location. That of the latter, however, is around 5mm regardless to the chemical reaction models. It is approximately a half of the experimental result.

With respect to the chemical reaction models, the reaction surface location of Arrhenius model is higher than that of equilibrium model by about 1mm. It is explained as follows. Sodium hydroxide (NaOH) and sodium oxide (Na_2O) concentration distributions near reaction surface are shown in Fig. 5. In the Arrhenius model, only the sodium hydroxide is produced according to Eq. (1). On the other hand, in the equilibrium model, sodium oxide is produced below the reaction surface where sodium is rich and the water vapor is lean. That it to say, more sodium is consumed in the equilibrium model than in Arrhenius model. This is why the reaction surface moves downward in equilibrium model.

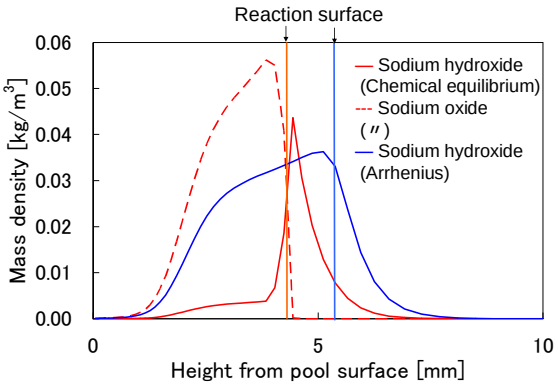

Fig. 5. Sodium hydroxide and sodium oxide concentration distributions near reaction surface

Next, let the authors discuss the concentration gradients of the water vapor and the sodium looking at Fig. 4. In the experiment, water vapor is supplied at 2.0 volumetric percent of the concentration. The water vapor concentration decreases linearly between 13-10 mm from the pool surface as shown in Fig. 4. Here, it is noted that there is no difference in concentration gradients of water vapor between the experiment and the simulation. In other words, the simulation reproduces the diffusion-controlled reaction and mass transfer process appropriately with regard to the water vapor. The reaction rate is controlled by mass transfer velocity. Meanwhile, the sodium saturated vapor pressure at the sodium pool temperature 820K is 1.38kPa. Therefore, the concentration of the sodium vapor at the pool surface is 3.3 volumetric percent (saturated condition) at the test pressure, 0.042MPa (= 42kPa). Whereas the sodium vapor concentration decreases between 0-3 mm linearly, the concentration gradient of the sodium becomes less steep from 3 mm to 10 mm. This fact suggests that the sodium is consumed before it reaches to the reaction

surface at 10mm above the sodium pool surface. The reaction takes place in water vapor rich and sodium vapor lean condition and the reaction rate in gas phase is relatively small near the reaction surface.

3.3 Aerosol Distribution in Experiment

In the experiment carried out in last year, detailed spatial distributions of the reaction products such as a sodium monomer, a sodium dimer, and aerosols are measured. The measurement methods of the sodium monomer, sodium dimer are CARS technique and Laser-Induced Fluorescence (LIF) technique, respectively. The aerosols diameter distribution is measured with Mie scattering and the aerosol volumetric distribution is measured by the Laser Induced Incandescence (LII) technique.

The volumetric concentration and the diameter distribution of the aerosols and the self-luminescence of the sodium are shown in Fig. 6. The peak of the Na self-luminescence corresponds to the light emission as shown in Fig. 3. As to the volumetric concentration, two peaks appear at 10 mm and 7-8 mm. The peak at 10 mm seems to correspond to the reaction surface shown in Fig. 4. Thus, it is obvious that the peak at 10 mm has something to do with the reaction products. Here, it is seen from Fig. 6 that the particle diameter becomes larger as the aerosol reaches to the pool surface. It is noted that the water vapor does not exist in the space below the reaction surface at 10mm. Therefore, it is reasonable to consider that the aerosol absorbs the sodium vapor on the surface

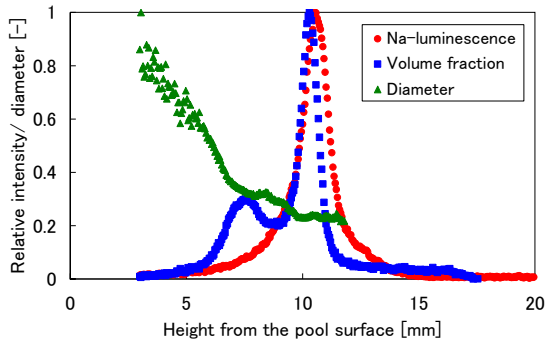

Fig. 6. The volumetric concentration distribution of the aerosols

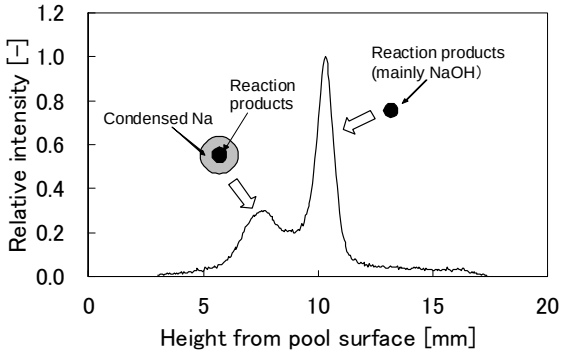

Fig. 7. The composition of the aerosols

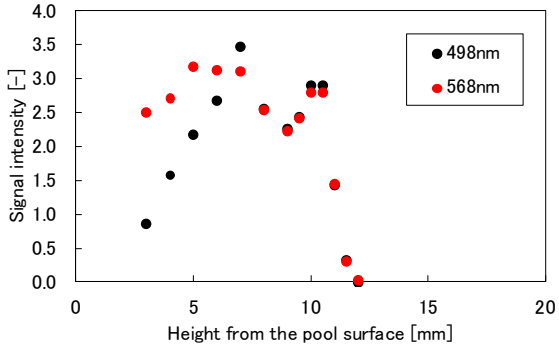

Fig. 8. Signal intensity distribution for irradiating 222nm laser beam

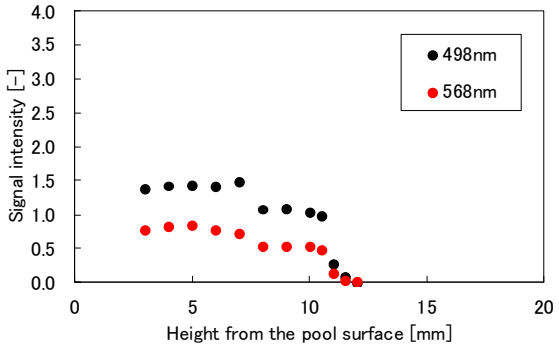

Fig. 9. Signal intensity distribution for irradiating 245nm laser beam

that results in the peak at 7-8 mm with larger diameter. The peak of the volumetric fraction in Fig. 6 corresponds to the sodium mist which kernel is the sodium hydroxide aerosol. The schematic of this idea is shown in Fig. 7.

The authors irradiated laser beams of 222nm and 245nm to investigate the reaction products. Figures 8 and 9 are signal intensity distributions of 498nm and 568nm wave length when 222nm and 245nm laser beams are irradiated. The intensity shown in Fig. 8 is a derivation from sodium dimer, sodium mist and sodium hydroxide. It is seen that two peaks are observed at 10 mm and 7 mm as in Fig. 8. Comparing Fig. 8 with Fig. 6, it is indicated that the peak at 10 mm is sodium hydroxide and the peak at 7 mm is sodium mist. On the other hand, the intensity of Fig. 9 is a derivation from sodium dimer, sodium mist and sodium oxide. It is also seen that the intensity peaks in some degree at 7 mm as well as Fig. 8. However, the obvious peak is not observed at 10 mm, the reaction region. In the experiments, namely, the authors have no the evidence that indicates the sodium oxide exists in the gas phase in the gas-phase reaction. Thus, the assumption that Arrhenius model has is valid.

The reaction products remained in the pool are analyzed after the experiments. At the peripheral zone of the pool, sodium hydroxide is observed. On the other hand, in the center of the pool, both sodium oxide and

sodium hydroxide are observed. The reaction products (mainly sodium hydroxide) settle by gravity and stayed in the pool. The sodium hydroxide settled at the pool peripheral remains as is because no sodium exists at the pool peripheral. The sodium hydroxide that settled at the pool center sinks to the pool bottom and stays in the sodium-rich condition. In this condition, the chemical reaction described in Eq. (2) may proceed. Thus, it is natural to consider that the sodium oxide observed in the pool bottom is formed when the sodium hydroxide settles to the pool (sodium rich environment).

4. Discussion Sodium Dynamics near Reaction Surface

In the experiment, the gas temperature is maximum at the sodium pool and the water vapor flow and the guard flow temperatures are lower than the sodium pool temperature. Fig. 10 shows a sodium saturated vapor concentration curve estimated based on the saturation pressure corresponding to the temperature distribution measured in the experiments. It is considered that the saturated sodium vapor evaporated from the pool condenses as it moves upward and the temperature decreases.

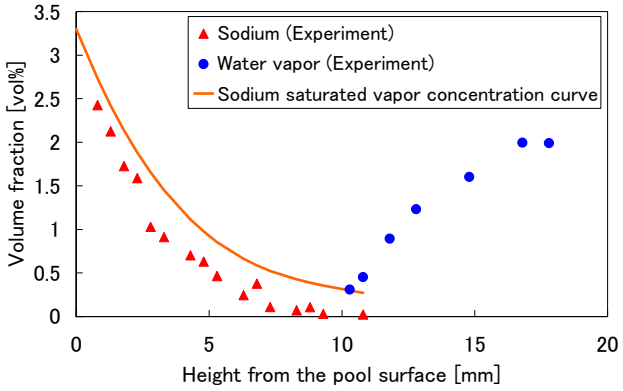

Fig. 10. Sodium saturated vapor concentration

It is seen from Fig. 10 the saturated sodium concentration curve is in accordance with the experiment. Consideration of the sodium condensation may explain the difference of the reaction surface between the simulation and the experiments as shown in Fig. 4. Also, the condensation of the sodium on the surface of the sodium hydroxide aerosol shown by the peak at 7-8mm in Fig. 7 is consistent with the present discussion. Although some modification of the test apparatus is required to increase the atmospheric temperature higher than the sodium pool temperature keeping the depressurized situation, an experiment at higher temperature at which the sodium condensation is not plausible is planned as the future work.

5. CONCLUSIONS

The mechanism of the SWR is researched by both the counterflow diffusion flame experiments and the numerical simulations. The computer program developed for the SWR is effectively used in the experiment design and the interpretation of the experimental results. The experiment in low-pressure condition enables the authors to measure the detailed distribution of the chemical species, temperature and aerosols.

In the present research, the authors observed two peaks at 10 mm and 7-8 mm in the aerosol volume fraction distribution. Whereas the former of the peaks derives from the reaction products (mainly sodium hydroxide), the latter of the peaks derives from the sodium mist caused by the sodium vapor condensation with the reaction products. The condensation is interpreted by sodium saturated vapor concentration curve.

Future works are the computer program improvement built in vapor pressure of sodium monomer and sodium dimer and sodium vapor condensation and the comparison of the experiment and numerical simulation. Through this process, the mechanism of the SWR in the gas-phase would be depicted.

NOMENCLATURE

A	frequency factor [-]
C_p	specific heat at constant pressure [J/kg/K]
C_u	Cunningham correction factor [-]
D_k	effective binary diffusivity of argon and chemical species k [m^2/s]
E	activation energy [J/mol]
g	gravitational constant [m/s^2]
k	reaction rate constant [m^3/mol/s]
$n(v)$	aerosol number density with its volume v [$1/cm^3$]
p	pressure [Pa]
Q_D	heat quantity transferred by diffusion [$J/m^3/s$]
Q_R	heat generation by chemical reactions [$J/m^3/s$]
R	gas constant [J/mol/K]
r	special coordinate in radial direction [m]
S	aerosol production rate [$1/cm^3/s$]
T	temperature [K]
t	time [s]
u	velocity in radial direction [m/s]
w	velocity in vertical direction [m/s]
Y_k	mass fraction of a chemical species k [-]
z	special coordinate in axial direction [m]

Greek Letters

β	aerosol coagulation rate [-]
γ	reaction rate [$mol/m^3/s$]
λ	thermal conductivity [W/m/K]
μ	viscosity coefficient [kg/m/s]
ρ	density [kg/m^3]

Subscripts

j	chemical species j

REFERENCES

Takata, T., Yamaguchi, A., *et al.* (2005). "Numerical Methodology of Sodium-Water Reaction with Multiphase Flow Analysis," *Nucl. Sci. Eng.*, **150**(2),

pp.221-236.

Takata, T., Yamaguchi, A., *et al.* (2009). "Computational Methodology of Sodium-Water Reaction Phenomenon in Steam Generator of Sodium-Cooled Fast Reactor," *J. Nucl. Sci. Technol.*, **46**(6), pp.613-623.

Yamaguchi, A., Takata, T., *et al.* (2006). "SODIUM-WATER REACTION AND THERMAL HYDRAULICS AT GAS-LIQUID INTERFACE: NUMERICAL INTERPRETATION OF EXPERIMENTAL OBSERVATIONS," *Proceedings of the 14th International Conference on Nuclear Engineering (ICONE14)*, Miami, Florida, USA, June 17-20.

Yamaguchi, A., Takata, T., *et al.* (2008). "NUMERICAL PREDICTION AND OPTIMIZATION OF DEPRESSURIZED SODIUM-WATER REACTION EXPERIMENT WITH COUNTER-FLOW DIFFUSION FLAME," *Proceedings of the 16th International Conference on Nuclear Engineering (ICONE16)*, Orland, Florida, USA, May 11-15.

Mitsutsuka, N. (1984). "ABC-ITNG CODE FEATURES," PNC-TN241-84-05, Power Reactor and Nuclear Fuel Development Corporation (PNC).

Okano, Y. (1999). "Development of Bi-Phase Sodium-Oxygen-Hydrogen Chemical Equilibrium Calculation Program (BISHOP) using Gibbs Free Energy Minimization Method," JNC-TN9400-99-071, Japan Nuclear Cycle Development Institute (JNC), [in Japanese].